Geophysical Research Letters

RESEARCH LETTER
10.1029/2023GL105868

Tropical Cirrus Are Highly Sensitive to Ice Microphysics Within a Nudged Global Storm-Resolving Model

R. L. Atlas[1,2], C. S. Bretherton[1,3], A. B. Sokol[1], P. N. Blossey[1], and M. F. Khairoutdinov[4]

[1]Department of Atmospheric Sciences, University of Washington, Seattle, WA, USA, [2]Laboratoire de Météorologie Dynamique/IPSL, École Polytechnique, Palaiseau, France, [3]Allen Institute for Artificial Intelligence, Seattle, WA, USA, [4]School of Marine and Atmospheric Sciences, Stony Brook University, Stony Brook, NY, USA

Key Points:

- Nudged global storm-resolving simulations are valuable for microphysics sensitivity studies
- Mean tropical longwave cloud radiative effect varies over 20 W m^{-2} depending on microphysics scheme
- Two-moment schemes outperform simpler one-moment and partial double-moment schemes, and P3 has the smallest longwave radiative bias

Supporting Information:

Supporting Information may be found in the online version of this article.

Correspondence to:

R. L. Atlas,
rachel.atlas@lmd.ipsl.fr

Citation:

Atlas, R. L., Bretherton, C. S., Sokol, A. B., Blossey, P. N., & Khairoutdinov, M. F. (2024). Tropical cirrus are highly sensitive to ice microphysics within a nudged global storm-resolving model. *Geophysical Research Letters*, *51*, e2023GL105868. https://doi.org/10.1029/2023GL105868

Received 3 NOV 2022
Accepted 10 DEC 2023

Abstract Cirrus dominate the longwave radiative budget of the tropics. For the first time, the variability in cirrus properties and longwave cloud radiative effects (CREs) that arises from using different microphysical schemes within nudged global storm-resolving simulations from a single model, is quantified. Nudging allows us to compute radiative biases precisely using coincident satellite measurements and to fix the large-scale dynamics across our set of simulations to isolate the influence of microphysics. We run 5-day simulations with four commonly-used microphysics schemes of varying complexity (SAM1MOM, Thompson, M2005 and P3) and find that the tropical average longwave CRE varies over 20 W m^{-2} between schemes. P3 best reproduces observed longwave CRE. M2005 and P3 simulate cirrus with realistic frozen water path but unrealistically high ice crystal number concentrations which commonly hit limiters and lack the variability and dependence on frozen water content seen in aircraft observations. Thompson and SAM1MOM have too little cirrus.

Plain Language Summary Recently, advancements in computing have made it possible for atmospheric scientists to simulate Earth's global atmosphere with higher resolution than ever before. This new generation of models, called global-storm resolving models, have a horizontal grid spacing of just a few kilometers, which permits the formation of thunderstorms. As a result, they simulate clouds more realistically than traditionally climate and weather models and are a great tool for diagnosing cloud biases in atmospheric models. Here, we run a single global storm-resolving model with four different representations of cloud physics called M2005, P3, SAM1MOM and Thompson. We evaluate simulated tropical cirrus, which are stratiform ice clouds at the top of the troposphere that reduce the amount of infrared radiation emitted by the Earth, with satellite and aircraft data to see which representations have the best performance. SAM1MOM and Thompson make too little cirrus causing too much infrared radiation to be emitted, M2005 makes too much cirrus, causing too little infrared radiation to be emitted, and P3 makes about the right amount.

1. Introduction

Tropical cirrus, which flow outward from deep convective cores (Deng et al., 2016) or form in-situ, absorb longwave radiation from Earth's surface and re-emit it at colder temperatures, thereby reducing outgoing longwave radiation and heating the atmosphere (Hartmann et al., 2001). Differences in the representation of cirrus in global climate models (GCMs), which stem from diverse model dynamics and physical parameterizations, are a major source of uncertainty in constraining the longwave radiative budget of the tropics and cloud climate feedbacks (Sherwood et al., 2020). Here, we quantify the variability in tropical longwave cloud radiative effect (CRE) that arises from differences in model microphysics across a set of global storm-resolving simulations (GSRMs), and we identify an important avenue for improving ice microphysics and more realistically simulating tropical cirrus.

Tropical cirrus are sensitive to the representation of deep convection and ice microphysics. These influences are difficult to disentangle in most global models, including high resolution GCMs, where both are parameterized. GSRMs, which typically have sub-5 km horizontal grid spacing and explicit rather than parameterized deep convection, provide a unique opportunity to isolate the influence of ice microphysics.

GSRMs are computationally expensive and thus are typically run for short durations ranging from a few days to a year. Comparisons of simulated CREs from short-duration simulations with climatological observations are sensitive to sampling bias. We address this issue by nudging our simulations to reanalysis to prevent the microphysics from feeding back onto the large-scale flow. This approach has many advantages including (a) allowing

comparisons with coincident real-world observations, (b) isolating the direct impact of differences in model microphysics on simulated cloud properties, and (c) reducing model spin-up time.

We run our nudged GSRM with four widely used microphysics schemes of varying complexity (single-moment, partial double-moment, and double-moment). We evaluate our simulations with remote sensing observations, including the newly released DARDAR-CLOUD v3.10 data set (Delanoë & Hogan, 2010), and in-situ observations, leveraging a new data set aggregating measurements from multiple aircraft campaigns that sampled cirrus clouds (Krämer, Rolf, Spelten, Afchine, et al., 2020).

2. Data

Four 5-day simulations are run with the Global System for Atmospheric Modeling (gSAM) (Khairoutdinov et al., 2022). They are set up identically, as described in Atlas et al. (2022), except that they are run with different bulk microphysics schemes: M2005 (Morrison et al., 2005, 2009), Thompson (Thompson et al., 2008), P3 (Morrison & Milbrandt, 2015) with one ice class, and SAM1MOM (Khairoutdinov & Randall, 2003). All schemes except SAM1MOM were originally developed for the Weather Research & Forecasting model (Skamarock & Klemp, 2008). The Community Earth System Model (Danabasoglu et al., 2020) and the Energy Exascale Earth System Model (E3SM) (Golaz et al., 2019) GCMs use microphysics schemes related to M2005, and the Simple Cloud Resolving E3SM Atmosphere Model GSRM (Caldwell et al., 2021) uses P3 microphysics.

Key differences in the representation of ice processes across the four schemes are summarized in Text S1 of Supporting Information S1. The simulations have approximately 4 km horizontal grid spacing in the tropics and about 500 m vertical grid spacing between 5 and 19 km. Deep convection is permitted but under-resolved using this grid spacing (Bryan et al., 2003). Simulations are initialized from ERA5 reanalysis (Hersbach et al., 2020) at 00 UTC 16 February 2018. We analyze days 2–5 of the simulations (17–20 February 2018) throughout this study, allowing one day for model spinup, long enough for cloud statistics to equilibrate (Atlas et al., 2022). Simulated temperature and horizontal winds (but not humidity or clouds) are nudged to ERA5 reanalysis with a damping timescale of 24 hr. We show that nudging reduces advective errors in gSAM in Text S2 of Supporting Information S1.

Simulated longwave and shortwave CREs are compared with coincident retrievals (overlapping the time period of the simulations) from Clouds and the Earth's Radiant Energy System level 3 data (Doelling et al., 2013; NASA/LARC/SD/ASDC, 2017), referred to hereafter as CERES. CERES has hourly temporal resolution and $1° \times 1°$horizontal resolution.

Retrieved frozen water content (FWC) from the DARDAR-CLOUD data set (Delanoë & Hogan, 2010) versions V2.1.0 and V3.10 (Cazenave et al., 2019) and the Cloudsat and CALIPSO Ice Cloud Property Product (2C-ICE) (Deng et al., 2015) version RF05 are used to evaluate simulated cirrus macrophysics. These retrievals have a horizontal resolution of 1.4 km, comparable to that of the simulations. The vertical resolution of DARDAR and 2C-ICE are 60 and 240 m, respectively. Because these retrievals are sparse in space and time and direct comparisons cannot be made for the simulated days, we use February data from the years 2007–2012.

Simulated microphysics are evaluated with in situ airborne observations of ice crystal number concentration (N_{ice}) and FWC from five aircraft campaigns, which are included in the "Microphysics Guide to Cirrus" (Krämer, Rolf, & Spelten, 2020), as described in Krämer, Rolf, Spelten, Afchine, et al. (2020). Text S3–S4 and Figures S4–S6 in Supporting Information S1 further discuss our use of DARDAR, 2C-ICE and the "Microphysics Guide to Cirrus."

3. Simulations Exhibit Wide-Ranging Tropical Longwave CREs

Figure 1 compares day 2–5 mean simulated CREs with CERES. Throughout this study, radiative fluxes are defined as positive downwards, so that negative CREs indicate energy lost from the Earth. Shortwave CRE biases (panel b) are largest and most scheme-dependent over the Southern Ocean, mainly due to differences in marine boundary layer clouds (Atlas et al., 2022).

In this study, we focus on the region between the horizontal parallel lines at 20°N and 20°S, hereafter referred to as "the tropics," where longwave CRE is highly sensitive to microphysics (panel a).

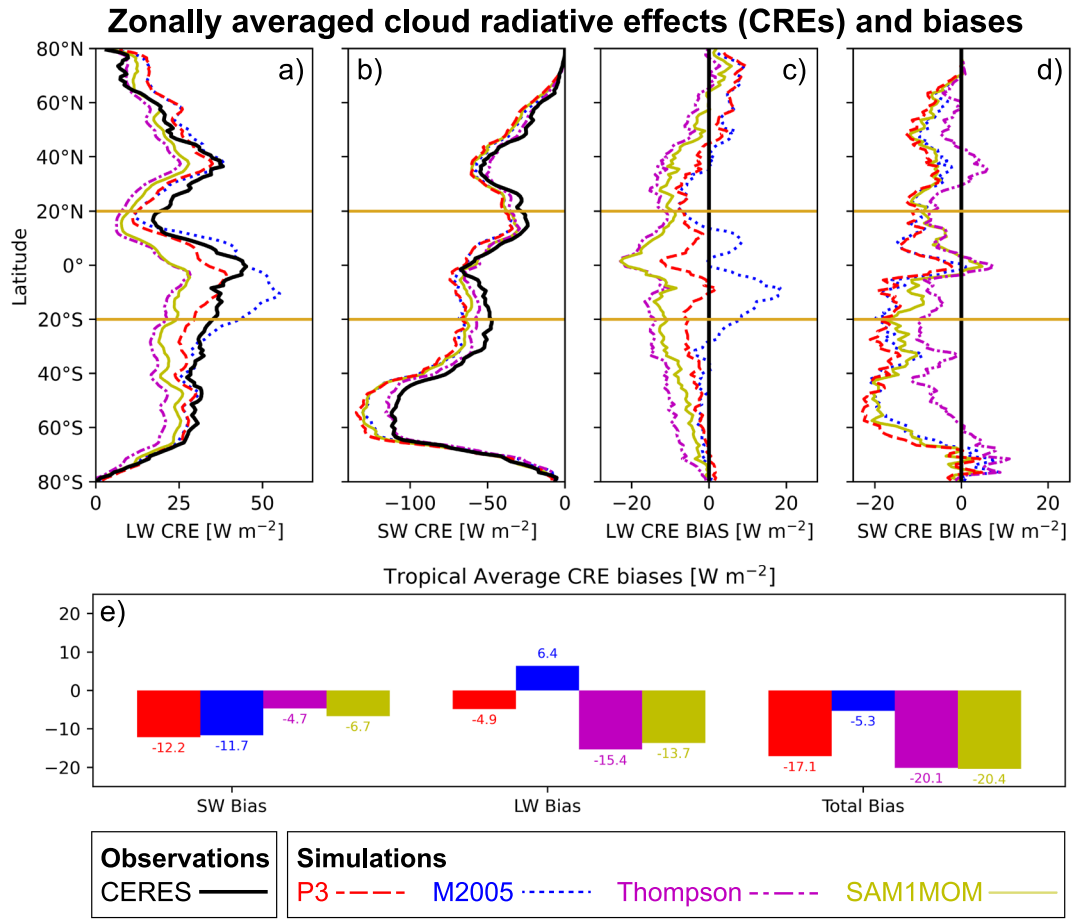

Figure 1. (a–b) Zonal average top of atmosphere cloud radiative effects (CREs) and (c–d) their biases versus CERES. Horizontal parallel lines delineate the tropical analysis region (20°S–20°N). (e) Tropical average cloud radiative effect biases for (left to right) shortwave, longwave, and total (shortwave + longwave).

Zonally-averaged longwave and shortwave CRE biases for each scheme are plotted on panels c–d. Panel e shows area-weighted tropical mean CRE biases for the simulations. Longwave and shortwave CRE biases vary over ranges of 21.8 and 7.5 W m^{-2}, respectively. While all simulations have a bright (negative) tropical shortwave CRE bias, the sign of the longwave CRE bias differs between M2005 and the other schemes. P3 has the least biased longwave CRE and M2005 has the smallest total CRE bias, which it achieves through compensating longwave and shortwave biases.

4. Variability in Macrophysical and Optical Cirrus Properties Lead to Diverse Longwave CREs

Figure 2 shows coincident snapshots at an arbitrarily chosen time of simulated frozen water path (FWP, the sum of the cloud ice, snow and graupel water paths) for columns containing high cloud, on the left, and biases in simulated longwave CRE, coarsened to a 1° × 1° grid, on the right. Columns with high cloud have a cloud top height (CTH) exceeding 10 km, where CTH is defined as the highest model level with FWC (the sum of the cloud ice, snow and graupel water contents) ≥ 10^{-4} g m^{-3} (the limit of lidar detectability as discussed in Text S3 of Supporting Information S1).

Animation S1 loops through versions of Figure 2 for each of the 96 hr of model output within days 2–5 of the simulations, showing that any hourly snapshot is representative of the entire 4 day period.

M2005 has the most areas with positive longwave CRE bias, which are typically coincident with anvil cirrus ($10 < \text{FWP} \leq 10^3$ g m^{-2}, magenta and orange colors). Thompson and SAM1MOM have negative longwave biases

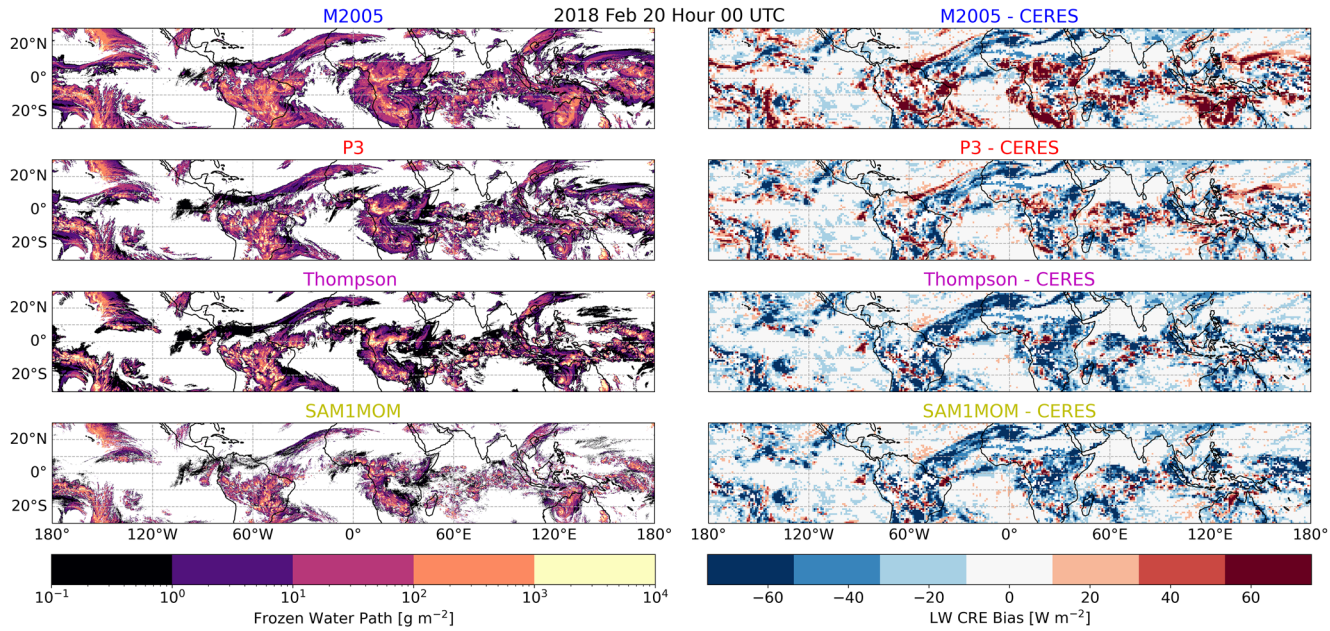

Figure 2. (left) Snapshots of simulated frozen water path for columns with CTH ≥ 10 km on the simulations' native grid. (right) Coincident snapshots of longwave cloud radiative effect bias compared to CERES on a coarsened 1° × 1° grid.

in most areas of thin cirrus (FWP ≤ 10 g m^{-2}, black and purple colors) and anvil cirrus. P3 has a mixture of positive and negative biases associated with thin and anvil cirrus, and the fewest areas with large biases of either sign.

The coarsened longwave CRE bias is sensitive to the amount of simulated cloud, and the optical thickness of simulated cloud. In Figure 3, we distinguish between the two, and we use CERES, DARDAR and 2C-ICE to provide observational constraints. The CALIPSO lidar used by DARDAR and 2C-ICE has greater sensitivity at night, during which it can detect FWCs ≥ 10^{-4} g m^{-3} (Text S3 in Supporting Information S1). Thus, we use DARDAR and 2C-ICE data from the nighttime A-train overpass, which crosses the equator at approximately 1:30 a.m. local time. For consistency, we also sample CERES and the simulations at night. FWCs < 10^{-4} g m^{-3} are filtered out of the simulations and satellite retrievals.

Figure 3a shows distributions of FWP from the simulations, two versions of DARDAR, and 2C-ICE. Figure 3b shows mean longwave CRE as a function of FWP. We do not show an observational comparison here because the retrieved FWP from DARDAR and 2C-ICE is 1D and cannot be matched with the coarsely gridded longwave CRE from CERES. Figure 3c shows the tail of the histogram of longwave CRE for the simulations, which is essentially the distributions in Figures 3a and 3b multiplied together. Only columns with CTH ≥ 10 km and grid cells with FWC ≥ 10^{-4} g m^{-3} are used in Figures 3a–3c. Figure 3d shows the same thing as Figure 3c but for coarsened simulation data and CERES. Only nighttime data are used for Figure 3.

The simulations and the two DARDAR data sets have unimodal distributions of FWP whereas 2C-ICE has a bimodal distribution. The discrepancy between DARDAR and 2C-ICE for FWP < 30 g m^{-2}, noted by Hong et al. (2016), emphasizes limitations on constraining FWP from CALIPSO in tropical cirrus too thin to be detected by CloudSat. Satellite retrievals from deep convective cores (FWP > 10^{3} g m^{-2}) are also uncertain (Delanoë & Hogan, 2010). Due to their variability, these data sets do not impose a tight constraint on the simulated FWP distribution, but it is useful to consider them as an envelope of plausible FWP distributions.

The simulations agree relatively well on the amount (Figure 3a) and longwave CRE (Figure 3b) of deep convective clouds. However, the simulations diverge for clouds with smaller FWP, including anvil cirrus and thin cirrus. P3 has more thin cirrus than the other simulations and most resembles 2C-ICE in cloud fraction and FWP distribution shape, albeit with a unimodal instead of bimodal distribution. M2005 has the most anvil cirrus and agrees best with DARDAR V2.1.1. DARDAR V3.10 has a larger cloud fraction than the other data sets and all of the simulations. Thompson and SAM1MOM have smaller cloud fractions and flatter FWP distributions than all of the observations.

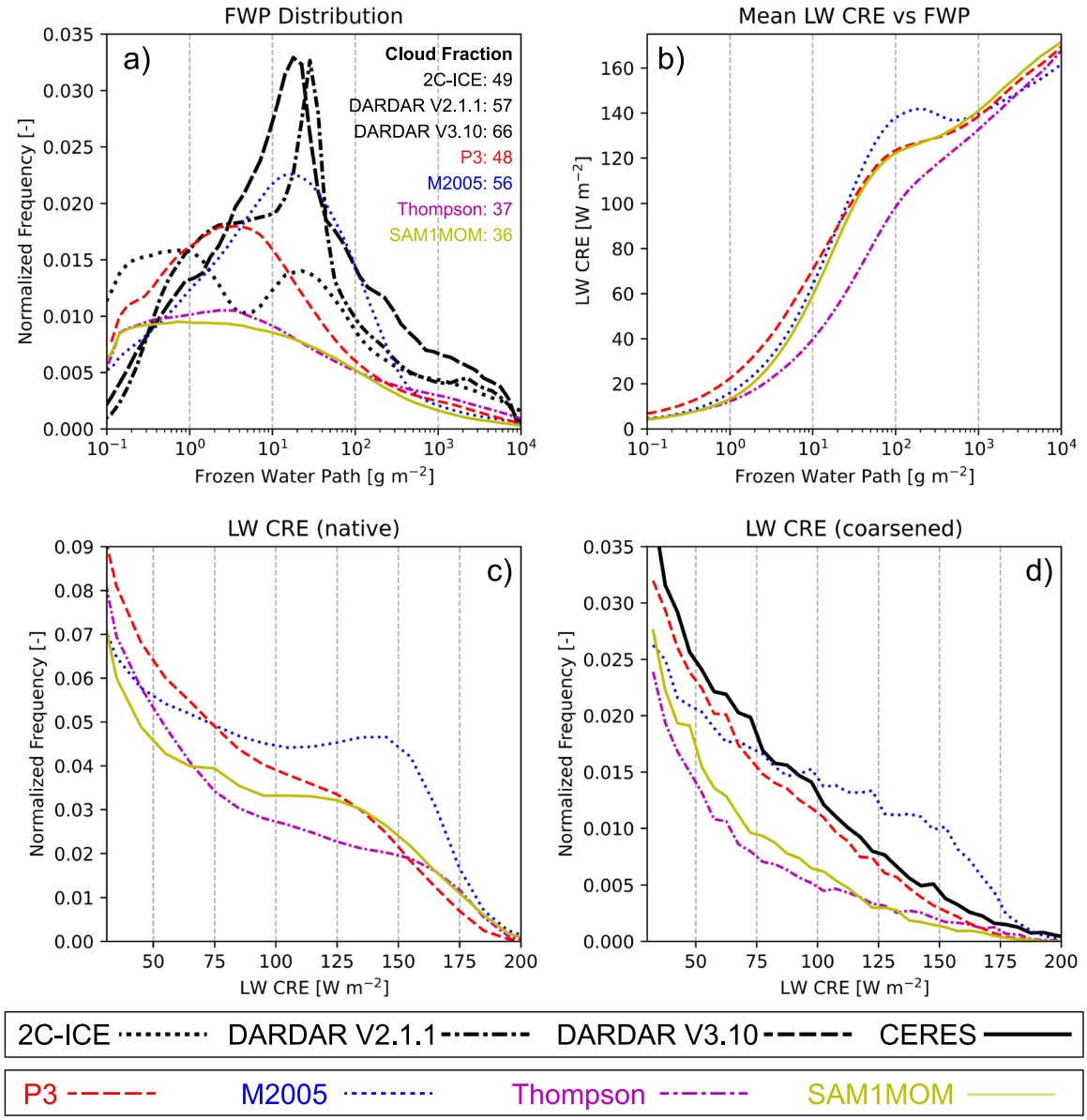

Figure 3. Tropical nighttime: (a) PDF of frozen water path (FWP) (b) Mean longwave cloud radiative effect (CRE) binned by FWP (c) PDF of longwave CRE, and (d) PDF of coarsened longwave CRE (1° × 1°). In panel (a), the area under the curves represents the fraction of high cloud columns, which is also printed on the plot. In panels (c and d), it represents the fraction of model columns, and 1° × 1°columns, respectively, with longwave CRE > 25 W m^{-2}.

M2005's FWP distribution peaks between 3 and 80 g m^{-2} (Figure 3a), and it has larger longwave CREs than the other simulations for cloudy columns with FWP between 20 and 700 g m^{-2} (Figure 3b), partially overlapping its FWP distribution peak. As a result, M2005 has a large peak in both its native and coarsened longwave CRE distribution between 100 and 175 W m^{-2} (Figures 3c and 3d), which is inconsistent with CERES. SAM1MOM and Thompson have fewer cloudy columns with FWPs between 0.7 and 100 g m^{-2} than the other simulations and the observed data sets (Figure 3a). Although SAM1MOM and Thompson have similar FWP distributions, Thompson has weaker longwave CREs for FWPs between 1 and 3,000 g m^{-2} (Figure 3b). As a result, SAM1MOM and Thompson both have too few columns with longwave CRE > 25 W m^{-2} compared to CERES, but Thompson is slightly more biased (Figure 3d). P3 has the most linear distribution of both native and coarsened longwave CRE (Figures 3c and 3d), due to having many clouds with FWP between 0.5 and 30 g m^{-2} (Figure 3a) and larger longwave CREs than the other simulations for FWPs between 0.1 and 20 g m^{-2} (Figure 3b). As a result, P3 agrees very well with CERES.

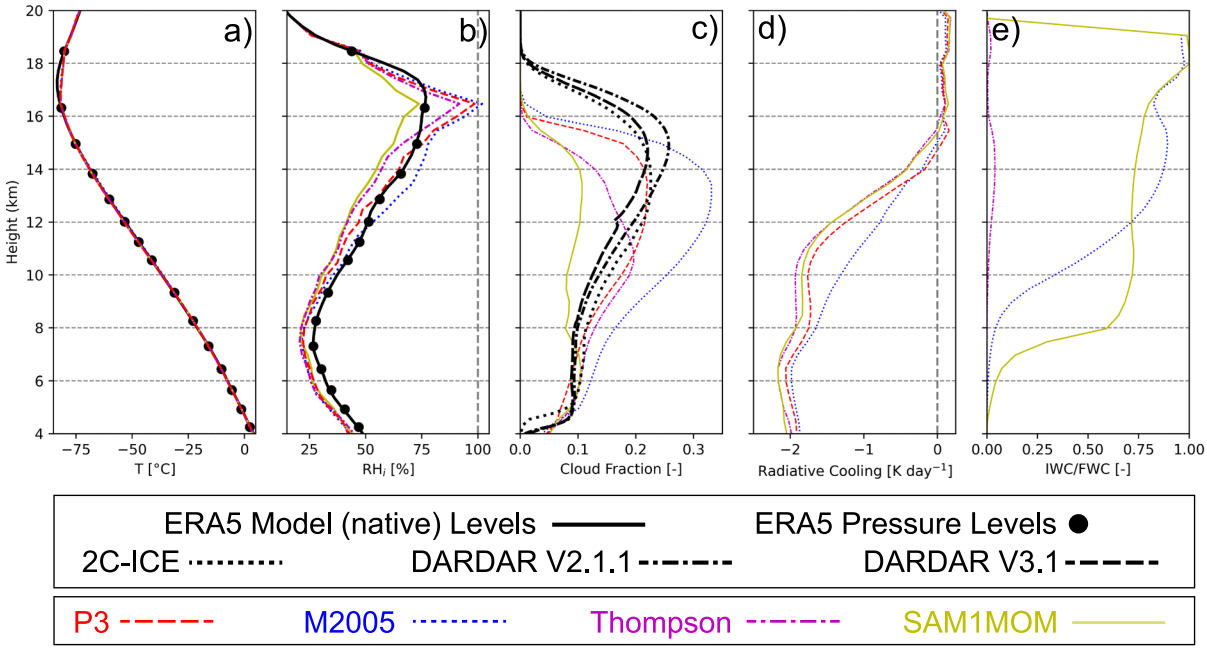

Figure 4. Vertical profiles of tropical nighttime (a) median temperature, (b) median RH_i, (c) cloud fraction (frozen water content (FWC) $\geq 10^{-4}$ g m^{-3} only), (d) mean longwave radiative cooling, and (e) IWC/FWC. We run P3 with one ice class so IWC/FWC cannot be computed.

P3 and M2005 have similar mean tropical longwave CRE biases, albeit of opposite signs (Figure 1). However, Figure 2 shows that P3 has typically smaller instantaneous longwave CRE biases than M2005, and Figure 3d shows that P3's mean bias comes from it slightly underestimating the frequency of coarsened longwave CREs > 25 W m^{-2}, but maintaining a realistic longwave CRE distribution shape. M2005 has an unrealistic longwave CRE distribution shape, and its moderate mean longwave CRE bias results from excessive longwave CREs > 100 W m^{-2} partially compensating deficient longwave CREs < 100 W m^{-2}.

Figure 4 compares simulated vertical profiles of thermodynamic and cloud properties with two ERA5 data sets, DARDAR and 2C-ICE. Figures 4a and 4b show profiles of median temperature and relative humidity with respect to ice (RH_i), respectively. Two versions of ERA5 are shown for comparison with the simulations: one on 137 native model levels (black lines), and the other on 37 interpolated pressure levels (black dots). In all simulations, temperature was nudged to pressure-level data, linearly interpolated to the gSAM model levels.

SAM1MOM has a lower median RH_i than the other simulations and ERA5, particularly above 14 km, possibly because it uses saturation adjustment for cloud ice, preventing RH_i from ever exceeding 100%. The importance of representing ice supersaturation for simulated cirrus properties has been noted in previous studies such as Lohmann et al. (2008). The other simulations have higher RH_i than ERA5 near the cold point, but ERA5 may be biased by its internal ice microphysical modeling assumptions in the tropical tropopause layer, where routine observations of the very low water vapor concentration are uncertain.

Figure 4c shows profiles of cloud fraction. Here, both DARDAR products and 2C-ICE are in better agreement and thus provide a tighter observational constraint on the simulations. For all simulations, the highest cloud tops are 2 km lower than observed. This is not due to either nudging or initialization with ERA5, as shown in Text S2 of Supporting Information S1.

Below 14.5 km, M2005's cloud fraction is much larger than the observations even though M2005 has a similar fraction of cloudy columns as DARDAR V2.1.1 (Figure 3a). This means that M2005 overestimates the geometrical thickness of ice clouds. Thus, although there may not be too many cloudy columns in M2005, cloudy columns contain too many cloudy grid cells on average. SAM1MOM underestimates cloud fraction above 8 km, where it has a nearly constant cloud fraction throughout the troposphere, in contrast to the other simulations and the observations. Thompson's cloud fraction peaks at 10.5 km, above which it has a much lower cloud fraction than the observations. P3 agrees best with the observations.

Figure 4d shows longwave radiative cooling profiles for the simulations. Throughout most of their depth, cirrus clouds reduce radiative cooling by absorbing upwelling longwave radiation. M2005 has up to 0.5 K day^{-1} less radiative cooling than the other simulations between 8 and 13 km due to its comparably large anvil cirrus coverage. Thompson and SAM1MOM, which have the smallest cirrus coverage, correspondingly have the strongest longwave cooling. These results are consistent with Hu et al. (2021).

In Section 3, we showed that mean tropical longwave CREs vary widely across the four simulations. In this section, we evaluated the distribution of tropical longwave CRE, and examined how it is shaped by the macrophysical and optical properties of the simulated clouds. M2005 is dominated by anvil cirrus (Figure 3a) with strong longwave CREs (Figure 3b) that are geometrically thicker than observed clouds (Figure 4c). As a result, its longwave CRE distribution is too heavily weighted toward longwave CREs > 100 W m^{-2} (Figure 4d). SAM1MOM has too few cloudy columns (Figure 3a) and too little cloud above 8 km (Figure 4c). Thompson has too few cloudy columns (Figure 3a), too little cloud above 10 km (Figure 4c), and the weakest longwave CREs for thin and anvil cirrus (Figure 3b). Both simulations have too few areas with longwave CRE > 25 W m^{-2}. P3 is dominated by thin cirrus (Figure 3a) and its height-resolved cloud fraction matches observations well (Figure 3b). As a result, its longwave CRE distribution shape agrees best with CERES.

Ice microphysics drives the differences discussed here because the size and shape of ice particles determines the optical properties of cirrus, and cirrus evolution and lifetime, by modifying key processes such as sedimentation. We begin to examine the influence of microphysics in Figure 4e, which shows the average mass of IWC (cloud ice only) divided by FWC (cloud ice + snow + graupel). We run P3 with one ice class so it is not shown here. Thompson's FWC is dominated by snow, unlike M2005 and SAM1MOM. It is likely that, in Thompson, excessively efficient autoconversion of cloud ice to quickly falling snow causes the altitude of peak cloud fraction to be biased low. In the next section, we evaluate the microphysics in M2005, Thompson and P3 with aircraft data.

5. Simulated Ice Crystal Populations Lack Observed Variability

We compare simulated N_{ice} and FWC with in situ airborne observations from five tropical field studies, synthesized in the "Microphysics Guide to Cirrus" (Krämer, Rolf, Spelten, Afchine, et al., 2020) (see also Section 2, Text S4 and Figure S6 in Supporting Information S1), which have been coarsened to 0.04 Hz to match the horizontal grid spacing of the simulations. Observations are from heights above 10 km, and latitudes between 20°S and 20°N; model histograms are from heights above 10 km within high-cloud columns from all post-spin-up output times (day and night).

Figure 5 shows 2D histograms of FWC and N_{ice} for M2005, P3, Thompson and in situ observations. SAM1MOM is omitted because it does not predict or estimate N_{ice}. N_{ice} and FWC for M2005 and Thompson include cloud ice, graupel and snow. Vertical lines overlaid on the 2D histograms show limiters specified within the microphysics schemes. These limiters are designed to prevent algorithms within the schemes from producing physically implausible results; if the limiter is frequently active, this suggests problems with parameterization assumptions made within the scheme and/or biases in model dynamics. Dotted lines show limiters on total cloud ice concentration and dashed lines show limiters on the concentration of ice particles produced through deposition nucleation, which is the dominant mode of nucleation within the temperature range investigated here. In Thompson, these two limiters are the same.

In M2005 and P3, most grid cells have values of N_{ice} that are very close to the smaller of these two limiters, which are 0.3 and 0.1 cm^{-3}, respectively. Both simulations have higher mean N_{ice} than the in situ observations and lack the observed variability in N_{ice} and dependence of N_{ice} on FWC. However, because the smaller limiter is three times smaller in P3 than in M2005, P3's ice crystal number concentrations are substantially closer to the observed mean.

Thompson has many grid cells with tiny FWC and N_{ice} and a subpopulation of grid cells dominated by snow (a large ratio of FWC to N_{ice}) as a result of efficiently converting most cloud ice to snow.

6. Conclusions

Tropical longwave CREs simulated by a global storm-resolving model are highly sensitive to ice microphysics, even when nudging is used to largely remove microphysics-dynamics feedbacks. Mean longwave CRE varies

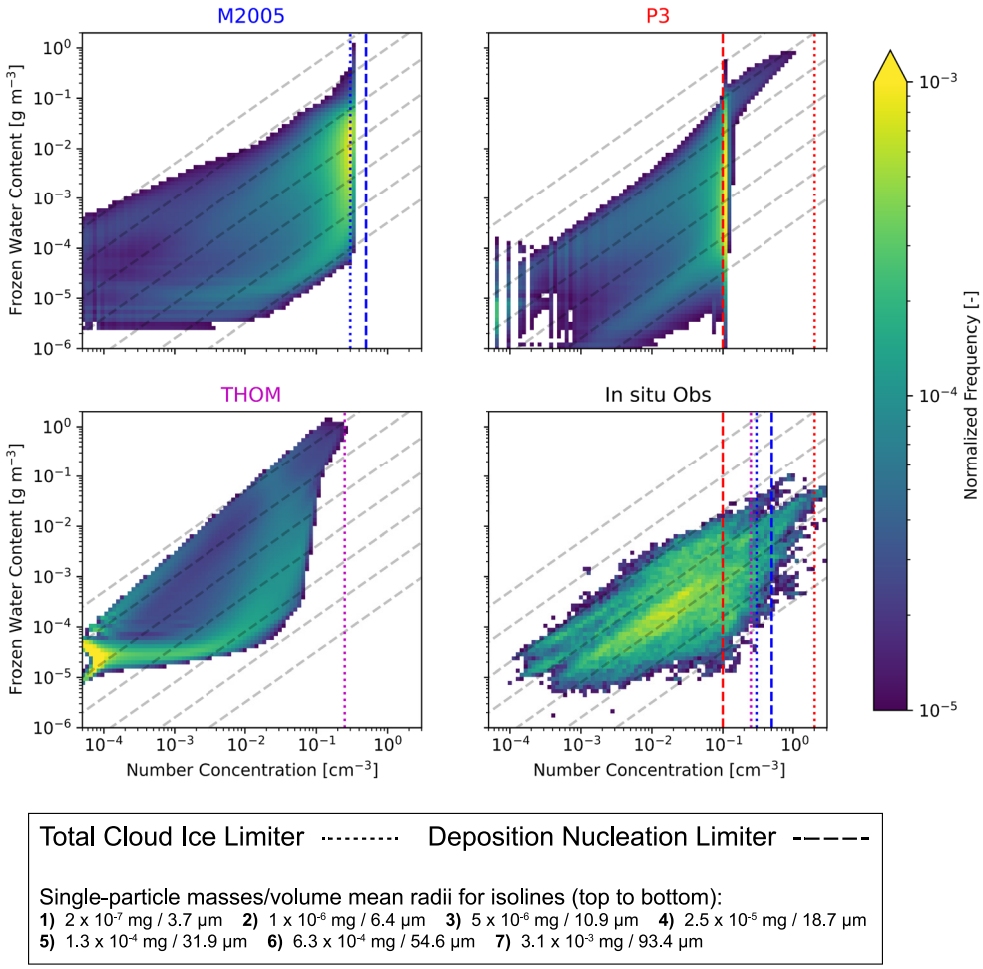

Figure 5. 2D histograms of frozen water content (y-axis, log-scale) and N_{ice} (x-axis, log-scale). Vertical dotted and dashed lines indicate limiters on total cloud ice number concentration and cloud ice particles formed through deposition nucleation, respectively. Diagonal dashed lines show isolines of volume mean radii which are listed below along with the corresponding particle mass, assuming uniformly sized spherical particles with solid ice density.

over a 22 W m^{-2} range across four simulations which differ only in their microphysical schemes, due to variability in cirrus amount, optical and geometric thickness, and ice crystal number and size. This shows the need for further improvement of ice microphysics parameterizations, even in GSRMs, for which the convective forcing of cirrus clouds is much more realistically represented than in present-day GCMs.

M2005 and P3 outperform Thompson and SAM1MOM as they have smaller mean longwave CRE biases, and more realistic distributions of FWP and vertical profiles of cloud fraction. Likely contributors to variability in cirrus and longwave CRE biases across the simulations are overly efficient autoconversion of cloud ice to snow in Thompson, saturation adjustment over ice in SAM1MOM, and simulated ice crystal number concentrations ubiquitously hitting arbitrary limiters within M2005 and P3. It is plausible that the differences in cloud properties and longwave CREs between M2005 and P3 are mainly due to their different limiters. M2005's overly large ice crystal number concentrations may lead to deficient sedimentation which allows the simulated clouds to grow thicker and last longer than they do in the real atmosphere. P3's smaller ice crystal number concentrations may better constrain the sedimentation to realistic values, allowing for a realistic profile of cloud fraction and longwave CRE distribution.

Ice crystal number concentrations hitting limiters can result from too strong ice crystal sources, too weak ice crystal sinks and/or errors in the resolved model dynamics. As M2005 and especially P3 are the most promising

schemes, and are used in several existing GCMs and GSRMs, an important avenue for future work is detangling these factors to precisely diagnose the cause of too high ice crystal number concentrations. It is worth considering that the schemes used here have been developed mainly for the purpose of simulating midlatitude or high latitude systems. Tropical high clouds likely have different dynamical and microphysical drivers. For example, convectively-generated gravity waves, which are only partly resolved by global storm-resolving models, are an important source of small-scale dynamic variability in the tropics (Atlas & Bretherton, 2023). Additionally, tropical high clouds exist at very cold temperatures and may be more influenced by homogeneous nucleation of aerosol, which is unrepresented in these schemes, and less influenced by heterogeneous nucleation.

Data Availability Statement

CERES (NASA/LARC/SD/ASDC, 2017), 2C-ICE R05 (https://www.cloudsat.cira.colostate.edu/data-products/2c-ice), DARDAR-CLOUD V2.1.0 and V3.10 (https://www.icare.univ-lille.fr/dardar/overview-dardar-cloud/), and the Microphysics Guide to Cirrus (Krämer, Rolf, & Spelten, 2020) are publicly available online. Simulated model output cannot be made available due to the experimental nature of the simulations and the large storage space required.

Acknowledgments
We acknowledge funding from U.S. National Science Foundation Grants OISE-1743753 (RLA and PNB) and AGS-1660604 (RLA, CSB and MFK), NASA Grant 80NSSC20K1613 (ABS), and high-performance computing support from Cheyenne (https://doi.org/10.5065/D6RX99HX) provided by NCAR's Computational and Information Systems Laboratory, sponsored by National Science Foundation, and we thank Blaž Gasparini and Maximilien Bolot for helpful discussions.

References

Atlas, R., & Bretherton, C. S. (2023). Aircraft observations of gravity wave activity and turbulence in the tropical tropopause layer: Prevalence, influence on cirrus clouds, and comparison with global storm-resolving models. *Atmospheric Chemistry and Physics*, *23*(7), 4009–4030. https://doi.org/10.5194/acp-23-4009-2023

Atlas, R., Bretherton, C. S., Khairoutdinov, M. F., & Blossey, P. N. (2022). Hallett-Mossop rime splintering dims cumulus clouds over the Southern Ocean: New insight from nudged global storm-resolving simulations. *AGU Advances*, *3*(2), e2021AV000454. https://doi.org/10.1029/2021AV000454

Bryan, G. H., Wyngaard, J. C., & Fritsch, J. M. (2003). Resolution requirements for the simulation of deep moist convection. *Monthly Weather Review*, *131*(10), 2394–2416. https://doi.org/10.1175/1520-0493(2003)131⟨2394:rrftso⟩2.0.co;2

Caldwell, P. M., Terai, C. R., Hillman, B., Keen, N. D., Bogenschutz, P., Lin, W., et al. (2021). Convection-permitting simulations with the E3SM global atmosphere model. *Journal of Advances in Modeling Earth Systems*, *13*(11), e2021MS002544. https://doi.org/10.1029/2021MS002544

Cazenave, Q., Ceccaldi, M., Delanoë, J., Pelon, J., Groß, S., & Heymsfield, A. (2019). Evolution of DARDAR-CLOUD ice cloud retrievals: New parameters and impacts on the retrieved microphysical properties. *Atmospheric Measurement Techniques*, *12*(5), 2819–2835. https://doi.org/10.5194/amt-12-2819-2019

Danabasoglu, G., Lamarque, J.-F., Bacmeister, J., Bailey, D. A., DuVivier, A. K., Edwards, J., et al. (2020). The community earth system model version 2 (CESM2). *Journal of Advances in Modeling Earth Systems*, *12*(2), e2019MS001916. https://doi.org/10.1029/2019ms001916

Delanoë, J., & Hogan, R. J. (2010). Combined CloudSat-CALIPSO-MODIS retrievals of the properties of ice clouds. *Journal of Geophysical Research*, *115*(D4), D00H29. https://doi.org/10.1029/2009JD012346

Deng, M., Mace, G. G., & Wang, Z. (2016). Anvil productivities of tropical deep convective clusters and their regional differences. *Journal of the Atmospheric Sciences*, *73*(9), 3467–3487. https://doi.org/10.1175/jas-d-15-0239.1

Deng, M., Mace, G. G., Wang, Z., & Berry, E. (2015). CloudSat 2C-ICE product update with a new Ze parameterization in lidar-only region. *Journal of Geophysical Research: Atmospheres*, *120*(23), 12198–12208. https://doi.org/10.1002/2015JD023600

Doelling, D. R., Loeb, N. G., Keyes, D. F., Nordeen, M. L., Morstad, D., Nguyen, C., et al. (2013). Geostationary enhanced temporal interpolation for CERES flux products. *Journal of Atmospheric and Oceanic Technology*, *30*(6), 1072–1090. https://doi.org/10.1175/jtech-d-12-00136.1

Golaz, J.-C., Caldwell, P. M., Van Roekel, L. P., Petersen, M. R., Tang, Q., Wolfe, J. D., et al. (2019). The DOE E3SM coupled model version 1: Overview and evaluation at standard resolution. *Journal of Advances in Modeling Earth Systems*, *11*(7), 2089–2129. https://doi.org/10.1029/2018MS001603

Hartmann, D. L., Moy, L. A., & Fu, Q. (2001). Tropical convection and the energy balance at the top of the atmosphere. *Journal of Climate*, *14*(24), 4495–4511. https://doi.org/10.1175/1520-0442(2001)014⟨4495:tcateb⟩2.0.co;2

Hersbach, H., Bell, B., Berrisford, P., Hirahara, S., Horányi, A., Muñoz-Sabater, J., et al. (2020). The ERA5 global reanalysis. *Quarterly Journal of the Royal Meteorological Society*, *146*(730), 1999–2049. https://doi.org/10.1002/qj.3803

Hong, Y., Liu, G., & Li, J.-L. F. (2016). Assessing the radiative effects of global ice clouds based on CloudSat and CALIPSO measurements. *Journal of Climate*, *29*(21), 7651–7674. https://doi.org/10.1175/jcli-d-15-0799.1

Hu, Z., Lamraoui, F., & Kuang, Z. (2021). Influence of upper-troposphere stratification and cloud–radiation interaction on convective overshoots in the tropical tropopause layer. *Journal of the Atmospheric Sciences*, *78*(8), 2493–2509. https://doi.org/10.1175/jas-d-20-0241.1

Khairoutdinov, M. F., Blossey, P. N., & Bretherton, C. S. (2022). Global system for atmospheric modeling: Model description and preliminary results. *Journal of Advances in Modeling Earth Systems*, *14*, e2021MS002968. https://doi.org/10.1029/2021MS002968

Khairoutdinov, M. F., & Randall, D. A. (2003). Cloud resolving modeling of the ARM summer 1997 IOP: Model formulation, results, uncertainties, and sensitivities. *Journal of the Atmospheric Sciences*, *60*(4), 607–625. https://doi.org/10.1175/1520-0469(2003)060⟨0607:crmota⟩2.0.co;2

Krämer, M., Rolf, C., & Spelten, N. (2020). The Cirrus Guide II in-situ aircraft data set [Dataset]. FZ-Juelich B2SHARE. https://doi.org/10.34730/266ca2a41f4946ff97d874bfa458254c

Krämer, M., Rolf, C., Spelten, N., Afchine, A., Fahey, D., Jensen, E., et al. (2020). A microphysics guide to cirrus – Part 2: Climatologies of clouds and humidity from observations. *Atmospheric Chemistry and Physics*, *20*(21), 12569–12608. https://doi.org/10.5194/acp-20-12569-2020

Lohmann, U., Spichtinger, P., Jess, S., Peter, T., & Smit, H. (2008). Cirrus cloud formation and ice supersaturated regions in a global climate model. *Environmental Research Letters*, *3*(4), 045022. https://doi.org/10.1088/1748-9326/3/4/045022

Morrison, H., Curry, J. A., & Khvorostyanov, V. I. (2005). A new double-moment microphysics parameterization for application in cloud and climate models. Part I: Description. *Journal of the Atmospheric Sciences*, *62*(6), 1665–1677. https://doi.org/10.1175/jas3446.1

Morrison, H., & Milbrandt, J. A. (2015). Parameterization of cloud microphysics based on the prediction of bulk ice particle properties. Part I: Scheme description and idealized tests. *Journal of the Atmospheric Sciences*, *72*(1), 287–311. https://doi.org/10.1175/jas-d-14-0065.1

Morrison, H., Thompson, G., & Tatarskii, V. (2009). Impact of cloud microphysics on the development of trailing stratiform precipitation in a simulated squall line: Comparison of one- and two-moment schemes. *Monthly Weather Review*, *137*(3), 991–1007. https://doi.org/10.1175/2008mwr2556.1

NASA/LARC/SD/ASDC. (2017). CERES and GEO-enhanced TOA, within-atmosphere and surface fluxes, clouds and aerosols 1-hourly Terra Edition4A [Dataset]. NASA Langley Atmospheric Science Data Center DAAC. https://doi.org/10.5067/TERRA+AQUA/CERES/SYN1DEG-1HOUR_L3.004A

Sherwood, S. C., Webb, M. J., Annan, J. D., Armour, K. C., Forster, P. M., Hargreaves, J. C., et al. (2020). An assessment of earth's climate sensitivity using multiple lines of evidence. *Reviews of Geophysics*, *58*(4), e2019RG000678. https://doi.org/10.1029/2019RG000678

Skamarock, W. C., & Klemp, J. B. (2008). A time-split nonhydrostatic atmospheric model for weather research and forecasting applications. *Journal of Computational Physics*, *227*(7), 3465–3485. https://doi.org/10.1016/j.jcp.2007.01.037

Thompson, G., Field, P. R., Rasmussen, R. M., & Hall, W. D. (2008). Explicit forecasts of winter precipitation using an improved bulk microphysics scheme. Part II: Implementation of a new snow parameterization. *Monthly Weather Review*, *136*(12), 5095–5115. https://doi.org/10.1175/2008mwr2387.1

References From the Supporting Information

Cooper, W. A. (1986). Ice initiation in natural clouds. *Meteorological Monographs*, *21*(43), 29–32. https://doi.org/10.1175/0065-9401-21.43.29

Jensen, E. J., Pfister, L., Jordan, D. E., Bui, T. V., Ueyama, R., Singh, H. B., et al. (2017). The NASA Airborne Tropical Tropopause Experiment: High-altitude aircraft measurements in the tropical western Pacific. *Bulletin of the American Meteorological Society*, *98*(1), 129–143. https://doi.org/10.1175/bams-d-14-00263.1

Pan, L. L., Atlas, E. L., Salawitch, R. J., Honomichl, S. B., Bresch, J. F., Randel, W. J., et al. (2017). The convective transport of active species in the tropics (CONTRAST) experiment. *Bulletin of the American Meteorological Society*, *98*(1), 106–128. https://doi.org/10.1175/bams-d-14-00272.1

Toon, O. B., Starr, D. O., Jensen, E. J., Newman, P. A., Platnick, S., Schoeberl, M. R., et al. (2010). Planning, implementation, and first results of the Tropical Composition, Cloud and Climate Coupling Experiment (TC4). *Journal of Geophysical Research*, *115*(D10), D00J04. https://doi.org/10.1029/2009JD013073

Wendisch, M., Pöschl, U., Andreae, M. O., Machado, L. A. T., Albrecht, R., Schlager, H., et al. (2016). ACRIDICON–CHUVA Campaign: Studying tropical deep convective clouds and precipitation over Amazonia using the new German research aircraft HALO. *Bulletin of the American Meteorological Society*, *97*(10), 1885–1908. https://doi.org/10.1175/bams-d-14-00255.1